Finding an Optimal Placement Depth for a Tidal In-Stream Energy Conversion Device in an Energetic, Baroclinic Tidal Channel

Mitsuhiro Kawase and Patricia Beba, School of Oceanography

Brian C. Fabien, Department of Mechanical Engineering

University of Washington, Seattle WA 98195 USA

Abstract

Hypothetical power dissipation by a tidal in-stream energy conversion device was calculated for Admiralty Inlet, Washington, a highly energetic entrance channel to Puget Sound and currently a candidate for tidal energy development. Power dissipation was calculated for a device of a given capacity as a function of hub height above sea bottom (z), using acoustic Doppler current profiler data taken in 2007 and 2009 at seven locations throughout the Inlet. At five of the seven locations, where the tidal currents were predominantly bi-directional, power dissipation density increased roughly as $\sim z^{\gamma}$, with the exponent γ narrowly ranging from 0.62 to 0.66, up to at least z = 18m. At two of the five sites where the water depth exceeded this substantially, power was found to increase further with z but at slower rates with γ = 0.19 and 0.42. The remaining two sites out of the seven were both close to shoreline features, and the currents deviated significantly from bi-directionality. At one of the two the power increased at a slower rate of γ = 0.35 – 0.5, while at the other the increase was faster with γ = 0.91 – 0.96. The increase in power with height at the bi-directional sites is faster than would be expected from the one-seventh power law applicable to turbulent channels. However, it is still slower than the likely increase in the cost of device foundation with height, which would at a minimum scale as $\sim z$ due to the cost of materials alone, and likely scale faster in order for the installation to withstand the overturning moment exerted by the tidal current. Thus, placing a tidal device high in the water column to exploit stronger currents may not be economically attractive, given that the device operator needs to recoup the higher cost of device foundation required.

Introduction

In a typical tidal channel, the tidal current has significant vertical shear. This is due primarily to the friction exerted by the bottom of the channel on the tidal flow, although presence of baroclinic exchange circulation as well as effects of wind at the surface can modify the shear profile of the tidal current significantly. Still, it is generally the case that higher current velocities, and therefore higher power densities, are found away from the channel bottom, further up in the water column. Hence it would appear desirable to place a tidal in-stream energy conversion (TISEC) device, such as a tidal turbine, high in the water column (provided it does

not interfere with shipping traffic). However, to support a tidal turbine high would require larger foundational structure: Not only is this simply due to greater height, but this is also necessary due to a requirement of greater mechanical stability needed to withstand the greater overturning moment exerted by the current. Thus it becomes a practical question for site developers how the power harvest and therefore revenue would depend on the device height above bottom; and how this scaling would compare with the scaling of installation cost; so that they can determine an optimal depth for turbine placement.

In the wind power industry, wind speed variation with height is typically characterized in terms of a power law (Spera and Richards, 1979; Johnson, 1985) with the exponent varying with factors such as height, time of day, season of the year, nature of the terrain, wind speeds, and temperature. For a steady flow of water in a channel with a free surface, the flow velocity is thought to increase with the height above the bottom according to a power law, with the exponent typically being one-seventh (Chanson, 2004). Such power-law profiles are often verified in field observations and come with some theoretical justification (De Chant, 2005; Cheng, 2007). However, in a tidal channel, both the pressure gradient and the along-channel flow vary periodically; with friction present, the phase of the current in the tidal cycle in the lower part of the water column leads the phases of the currents higher up (Proudman, 1953; Bowden et al., 1959; Prandle, 1982a,b). As a result, a single power-law profile that would represent all phases of the tide does not exist. Further, in coastal waters stratification in density is often present, with fresh river water lying over a layer of saline water from the sea. Stratification modifies the character of turbulence in the water column and further affects the profile of tidal currents (Maas and van Haren, 1987). Finally, in an estuarine channel there is lateral as well as vertical density contrast between the fresh and the marine waters. The former contrast, coupling to the strain due to the sheared tidal current, generates periodically varying vertical stratification and introduces ebb-flood asymmetry to the current profile (Simpson and Souza, 1995). Thus, the vertical profile of the tidal current in a stratified estuary requires a fairly complex characterization. Understanding tidal variability in the presence of vertical and horizontal stratification is an area of active oceanographic research.

In the meantime, a site developer may obtain the necessary information on the vertical current profile for an optimal placement of the device from a long-term current measurement at the proposed site of device installation. Quantitative measurements of vertical structure of ocean current are now done routinely using an acoustic Doppler current profiler (ADCP). In this study, such current data from several proposed sites for tidal energy development at the mouth of a large fjord estuary are used to characterize how the power extraction potential depends on depth, and to explore an optimal placement strategy for a device.

Data

Observations of tidal currents used in this study are taken in the Admiralty Inlet, Washington (Figure 1), an energetic tidal channel currently considered for tidal

energy development. Admiralty Inlet connects the main body of Puget Sound, a large fjord estuary whose watershed basin contains the Seattle metropolitan area, with the Strait of Juan de Fuca and the Pacific Ocean beyond. It is the main conduit of exchange between Puget Sound and the outside, whether it is water, water-borne organisms such as fishes, or shipping traffic (Barnes and Ebbesmeyer, 1978; Cannon, 1983; Strickland, 1983). A recent one-dimensional modelling study of Puget Sound (Polagye, et al., 2009) indicates that a tidal cycle-average power generation of 200MW may be possible in Admiralty Inlet with a Sound-wide reduction in tidal amplitude of approximately 5%, about one-sixth of the current average energy demand of Seattle. Modelling (Kawase and Thyng, 2010) indicates that the speed of tidal currents in the Inlet frequently reach and exceed three meters per second; density stratification is highly variable, but never totally absent (Moore, et al., 2008).

Seven acoustic Doppler current profiler (ADCP) data sets from Admiralty Inlet, Washington, taken in 2007 and 2009, are used in this study (Table 1, Figure 1). They are a subset of the data described in Gooch et al. (2009). Three of the data sets are from the north end of Admiralty Inlet and are in relatively deep waters. Two were taken in the summer of 2007 by Evans-Hamilton, inc. as part of Snohomish Public Utility District's siting study for a pilot-scale tidal power installation; the third, in the spring of 2009 by the scientists from the Northwest National Marine Renewable Energy Center. The remaining four data sets are from the western side of the Inlet adjacent to Marrowstone Island; these are taken as part of siting study for U.S. Navy's tidal power demonstration project.

Tidal currents in Admiralty Inlet are of mixed character with periods of strong diurnal inequality (profiles from Admiralty Head 2007 data is shown as a representative case in Figure 2). Surface currents routinely reach the maximum of 3 m/s or greater. The vertical current profile is highly variable and defies a simple power law characterization (Gooch et al., 2009); in the example shown in Figure 2, only the peak flood profile agrees well with the one-seventh law.

Methods

In the following, we consider the case of a single, isolated turbine placement. We assume that the turbine does not significantly alter the large-scale flow regime such that the impact of extraction must be considered in resource assessment (Garrett and Cummins 2005, 2008; Polagye et al, 2008). Optimal placement of an array of turbines, including optimal placement in the vertical, will be addressed in future studies.

Instantaneous power generated by a tidal turbine of diameter D and an efficiency factor F_E in a stream of speed u is given by the formula (see Fig.3)

$$P = \begin{cases} 0, & u < u_C \\ \dfrac{\pi D^2 F_E \rho_W u^3}{8}, & u_C \le u \le u_R \\ \dfrac{\pi D^2 F_E \rho_W u_R^3}{8} \equiv P_R, & u \ge u_R \end{cases} \quad (1)$$

where ρ_W is the density of the estuarine water (here taken to be 1024 kilograms per cubic meter for a typical brackish water value), u_C is the cut-in speed below which the turbine does not turn, and u_R is the rated speed, above which the turbine turns at a constant rate and the power output also becomes constant. P_R is the rated power of the device. For our calculation, u_C is taken to be 0.5 meters per second.

The rated speed u_R is varied over a range from 1 meters per second to 2.5 meters per second. For each rated speed, the instantaneous power output at each ADCP depth bin is calculated using above formula and then averaged over the period of the ADCP record. The resultant average power output

$$\overline{P}(z,u_R) \equiv \frac{1}{T}\int_T P dt \quad (2)$$

is then divided by the rated power P_R to obtain the capacity factor F_C as a function of hub height z and rated speed u_R:

$$F_C(z,u_R) \equiv \overline{P}/P_R \quad (3)$$

This function, in turn, is inverted for u_R to obtain the rated speed, and thus the average and the rated power, for a given capacity factor. We consider capacity factors of 30% (F_C = 0.3) and 35% (F_C = 0.35). Finally, the average and the rated power are normalized by dividing with the turbine cross-sectional area $\pi D^2/4$ and the efficiency factor F_E, and thus are expressed in terms of device-independent (apart from rated speed) power density, whose unit is watts per square meter (W/m^2).

Results

In general, at a given hub height, the higher the capacity factor F_C the lower the rated speed u_R is (Figures 4 and 5), since the device is operating at the rated power production for a longer fraction of time. For a given rated speed, higher F_C values (higher average power) are seen higher up in the water column, as expected. For the deeper ADCP sites in Admiralty Inlet, commercially desirable capacity factors of thirty to thirty-five percent can be attained with rated speeds of 1.3 to 2 meters per second, depending on the hub height. At these deeper stations the capacity factor, first increasing rapidly with the hub height, then increases steadily but more slowly through the rest of the water column. The transition between the two regimes appears to occur over fifteen to thirty meters above the bottom; this may signify the top of a bottom boundary layer.

Rated speed u_R (Figure 6) and average power dissipation density (Figure 7) for F_C = 30% and 35% both show increase with hub height. The transition from the bottom boundary layer to the water column interior, mentioned above, is recognizable in the three deep profiles. At the four Marrowstone Island locations, the water appears shallow enough that the entire water column is within the boundary layer where power increase with hub height is rapid.

For the scaling arguments to be presented later, for the purpose of finding an optimal placement depth, it is useful to represent the height dependence of power density in terms of a power law: $\overline{P} \sim z^{\gamma}$. Best-fit γs for our profiles are calculated and tabulated in Table 2. For the three deeper stations, because of the transition from the boundary layer to the interior, separate γs are calculated for each and listed along with the approximate height of the boundary layer. For five of the seven profiles, the γ values for the bottom boundary layer (the Marrowstone Island profiles are all assumed to be within the bottom boundary layer) are very close to each other, ranging from 0.6157 (30%) and 0.6165 (35%) for the 2007 Admiralty Head profile to 0.6552 (30%) and 0.6572 (35%) for the Marrowstone Island D9 profile. The two remaining profiles, the 2009 Admiralty Head and the Marrowstone Island C5, are both from locations showing moderate to large flood-ebb asymmetry in the current (Gooch, et al., 2009) and may have been influenced by nearby shoreline features; exponents for these sites are both smaller and larger than for the remaining sites, respectively. Profiles in the upper part of the water column at the deeper sites show smaller exponent values but these values vary widely, from 0.189 (30%) and 0.203 (35%) for the 2007 Point Wilson profile to 0.4919 (30%) and 0.504 (35%) for the 2009 Admiralty Head profile.

Comparison with estimates based on cross-sectionally averaged velocities

The above calculations were done for each ADCP depth bin, with the assumption that the velocity there is representative of the velocity encountered by a tidal turbine whose hub is at the same height as the bin. More realistically, the turbine would sample the flow throughout the diameter of its propeller. There may be considerable current shear across the face of the propeller, especially as the turbine diameter increases. Thus there may be errors in power calculations based on velocities at the hub height alone. The ADCP data does not sample current variations in all dimensions (horizontal as well as vertical). Nevertheless, we have repeated the capacity factor and the average power calculations with velocities averaged over the cross-sectional area of a disk centered at the hub height, in order to ascertain how significant the velocity variance over the face of the turbine could be for power estimations. Turbine diameters of 5, 10 and 15 meters have been tried.

Cross-sectional averaging results in little changes in the estimated capacity factor and rated speed/power. As an example, power dissipation profiles for the 2007 Point Wilson data set is shown together with relative difference between local and cross-sectionally averaged estimates (Fig. 8). Only towards the bottom is there significant difference in average power dissipation density, and only for the largest diameter (-3.3% at this location). Profiles from other ADCP locations show similar

small differences; the largest relative difference was seen in the Marrowstone Island D9 data for a turbine diameter of 15m (-5.1%). However, this and other Marrowstone Island locations are so shallow that placing a 15m turbine would result in very little navigational clearance at the top. Placement of a large turbine in such a location, if at all possible, would be severely limited by the space constraint and not by the potential for power harvest.

The small difference between non-averaged and averaged estimates would be expected if, to the first approximation, current variability across the face of the turbine was linear so that the variability cancels out upon averaging and higher order effects are small. The tendency for the cross-sectional averaged power to be lower than the value at the center is consistent with the convex curvature of the height dependence of speed.

While it is straightforward to calculate a cross-sectionally averaged speed and use it in the power calculation, using local speed values is convenient in that we need not presuppose the diameter of the device. Our calculations indicate that estimating power density from the local speed and then multiplying it with the cross-sectional area of the turbine, as well as with the device efficiency, should give a sufficiently accurate estimate of power extraction by the turbine for planning purposes.

Discussion

Comparison with estimates from power-law profiles

ADCP current profiles are for specific geographic locations, and these may not be readily available for a given region where tidal energy development is contemplated. Information about currents with explicit spatial coverage may be available, but these are typically very limited in the vertical coverage. In some cases, only information about currents at the sea surface may be available, either from a compilation of data assembled for navigational purposes or from a high-frequency radar coverage; in other cases outputs of a two-dimensional tidal model may be available, but such a model predicts only depth-averaged currents. It may be necessary to do the initial resource assessment using such limited information.

Turbulent channel flow often shows a vertical speed profile that is proportional to the one-seventh power of the height above the bottom; such dependence has been theoretically justified also (De Chant, 2005). Accordingly, we generated speed profiles that assume this power-law dependence on height above the bottom and which match the ADCP speed either at the top of the water column or in the depth-average sense. (The former was matched at the topmost ADCP bin for each profile where reliable data was consistently available. Although this is not strictly at sea surface, the difference – at least for the purpose of our calculations – was presumed small. As for the latter, at all locations, there is a significant gap between the sea floor and the first consistently usable ADCP bin. However, we do not have means of determining the current profile in the missing part of the water column, so we have kept the averaging to within the depth range where reliable data was consistently available. Because currents in this gap are expected to be weaker than those in the

overlying water column, our estimate of the depth-averaged current speed is likely an overestimate.)

We repeated our capacity factor and power density calculations using these profiles to see how well the power-law assumption can capture the vertical profile of the available power (Fig. 9 and 10). Agreement between the ADCP and the one-seventh law calculation varies from one location to the other, with the 2007 Admiralty Head data showing a very good agreement except the lowest part of the water column; overall, however, it appears that the one-seventh law profile results in an overestimate of power, especially near bottom. This is more clearly seen in the plots of the relative disagreement between the ADCP-based and the power law-based calculations (Fig. 11 and 12). Using the power law results in anything from 20% to 80% overestimate of the power at the lowest level of the water column. One exception to this is the 2009 Admiralty Head data, where a power law-based estimate is lower than the ADCP estimate, as would be expected from the exceptionally large γ at this location.

Gooch et al. (2009) analyzed the power-law dependence of individual ADCP profiles and concluded that, while there is enormous variability from one profile to the next, on average the velocity increase with height is steeper than the one-seventh power law would predict. This would certainly lead to a steeper decay of power with depth than would be expected from a one-seventh law profile. As a final exercise we generated power-law speed profiles with an exponent that is the inverse-average of the exponents estimated by Gooch et al. (2009) for our ADCP data ($\gamma = 1/5.64 = 0.177$). For the three profiles from the central Marrowstone Island location and especially when the speed is matched to the data at the surface, this power law has resulted in a very good estimate of the power density profile (Fig. 13 and 14; only the 30% capacity factor case is shown). Even the large overestimate of the north Marrowstone Island C5 data has been brought down. As for the deeper stations, the near-bottom power estimates for the 2007 Admiralty Head data and the 2007 Point Wilson data have improved although the overall agreement for the former, as well as that for the 2009 Admiralty Head, has deteriorated.

When the profiles are matched to the depth-averaged speed, the result is a consistent overestimate; this is likely due to the overestimate of the vertical average velocity itself because of the limited range of the ADCP profile as mentioned above. While the number of cases considered in the present study is small and they are confined to a single geographical region, it seems promising that for locations where the current is dominantly bi-directional a good estimate of power profile from an empirical power law current profile can be obtained. If universality of such a power law for an energetic baroclinic tidal channel can be established, it could be a useful aid to evaluating tidal energy resource in a channel where depth profiles of currents are not readily available.

Comparison with scaling of installation cost with hub height

At the moment, the economics of electricity generation using tidal turbines is yet to be known; hence the following discussion of the optimal turbine height is made

necessarily in the abstract, and should be considered an example of how to formulate an argument rather than a definitive answer to such a question.

Since most currently envisioned tidal turbine systems are bottom-mounted, we assume this is the case in our analysis. It is possible that, in future, a mounting system using a surface barge moored to the sea floor with the turbine attached underneath can be developed. Such a configuration may have advantages in installation and maintenance costs, and may alter the scaling argument presented here (Eltaher, et al., 2003; Wayman, 2006). Assume the total revenue over the lifetime of the installation is given by

$$R = A\overline{P} \equiv Bz^{\gamma} \tag{4}$$

where A is average price of electricity times device lifetime. Also assume the expenditure associated with the device (installation and maintenance) to scale as

$$E = E_1 + E_2 z^{\delta} \tag{5}$$

Then the profit (gain) from the turbine with hub height z over the lifetime would be

$$G(B,E_1,E_2,z) \equiv R - E = Bz^{\gamma} - E_1 - E_2 z^{\delta} \tag{6}$$

The optimum device height above bottom for maximum profit would be

$$z_O = \left(\frac{\gamma B}{\delta E_2}\right)^{\frac{1}{\delta-\gamma}} \tag{7}$$

and the associated profit would be

$$G_O = \frac{\delta-\gamma}{\gamma}\left(\frac{\gamma}{\delta}\right)^{\gamma/(\delta-\gamma)} \frac{B^{\delta/(\delta-\gamma)}}{E_2^{\gamma/(\delta-\gamma)}} - E_1 \tag{8}$$

If $\delta > \gamma$ (a likely scenario), then z_O would indeed be the hub height for maximum profit. If on the other hand $\delta < \gamma$ (i.e. power output increases faster than expenditure with hub height), then z_O would be a *minimum* and G_O will be negative (a loss). In this case, it would be best to place the hub at the maximum possible hub height H_{Max} consistent with surface clearance and non-interference with vessel traffic (among other concerns) for the location, provided that $G(B, E_1, E_2, H_{Max}) > 0$ so that the turbine can turn profit.

Going back to the case of $\delta > \gamma$, it is possible that z_O would exceed H_{Max}. In this case, we can expect maximum profit to occur at H_{Max}, again provided that $G(B, E_1, E_2, H_{Max}) > 0$; otherwise the turbine would be uneconomical.

It is likely the cost of device foundation with height would, at a minimum, scale as $\sim z$ ($\delta = 1$) due to the cost of materials alone, and likely scale faster in order for the

installation to withstand the overturning moment exerted by the tidal current. Assuming $\gamma = 0.62$ for our representative case and $\delta = 1$,

$$z_O = 0.28\left(\frac{B}{E_2}\right)^{2.6} \tag{9}$$

and the associated profit is

$$0.28\frac{B^{2.6}}{E_2^{1.6}} - E_1 \tag{10}$$

The optimal placement depth depends sensitively on the average price of electricity over the installation lifetime – a volatile quantity that may be difficult to estimate on a sound basis. However, if one could settle on a range of possible values for B from B_{Min} to B_{Max}, say, one might proceed with formulating a placement strategy as follows. First, in order to guarantee that the turbine can turn a profit, it is necessary that either $G(B_{Min}, E_1, E_2, z_O) > 0$ or $G(B_{Min}, E_1, E_2, H_{Max}) > 0$. If the first condition is met, one can define a height range for profitability $[z_{Min}, z_{Max}]$ such that $G(B_{Min}, E_1, E_2, z) > 0$ for $z \in [z_{Min}, z_{Max}]$ (z_{Max} could be H_{Max}). Within this range, consider how the profit would depend on the average price of electricity, i.e. B. With increasing B, the profit increases linearly such that

$$\frac{\partial G}{\partial B} = z^{\gamma} \tag{11}$$

Thus the rate of increase is faster for higher hub heights; this would mean that, within the range of profitability, it would be advantageous to bias the turbine placement higher in the water column so that higher electricity prices would result in proportionately greater profit margins (see Figure 15 for a schematic illustrating this point). If $z_O > H_{Max}$, then it would be the most advantageous to place the turbine as high as possible in the water column.

Conclusions

The simple analysis presented here indicates that, in this particular tidal channel, power dissipation by a tidal turbine can increase with height above bottom faster than expected from a one-seventh power law profile. Conversely, one-seventh power law profiles fitted to the observed surface current would likely give an overestimate of power potential in the currents deeper down. Still, the rate of increase with height is less than the expect increase in the installation cost with the height; a careful economic analysis, based on credible projections of the price of electricity into the future among other factors, will be required before attempting to place a tidal turbine as high as possible in the water column.

Acknowledgments

The authors appreciate provision of ADCP data as well as technical discussions with Sam Gooch, Brian Polagye and Jim Thomson of NNMREC and Dallas Meggitt of

Sound and Sea Technology. During preparation of this document, Mitsuhiro Kawase was hosted at National Oceanography Centre, Southampton, United Kingdom. This material is based upon work supported by the Department of Energy under Award Number DE-FG36-08GO18179.

References

Barnes, C.A. and C.C. Ebbesmeyer, 1978. Some aspects of Puget Sound's circulation and water properties. In Estuarine Transport Processes, B. Kjerfve (ed.), University of South Carolina Press, Columbia, South Carolina, 209-228.

Bowden, K.F., L.A. Fairbairn and P. Hughes, 1959. The distribution of shearing stresses in a tidal current. Geophysical Journal of the Royal Astronomical Society, 2, 288-305.

Cannon, G.A., 1983. An overview of circulation in the Puget Sound estuarine system. NOAA Technical Memorandum ERL PMEL-48, 30pp.

Chanson, H., 2004. The hydraulics of open channel flow: An introduction ; basic principles, sediment motion, hydraulic modelling, design of hydraulic structures. Oxford [UK]: Elsevier Butterworth Heinemann.

Cheng, N.-S., 2007. Power-law index for velocity profiles in open channel flows. Advances in Water Resources 30(8), 1775-1784.

De Chant, L.J., 2005. The venerable 1/7th power law turbulent velocity profile: a classical nonlinear boundary value problem solution and its relationship to stochastic processes. Applied Mathematics and Computation, 161 (2), 463-474.

Eltaher, A., Y. Rajapaksa, and K.-T. Chang, 2006. Industry Trends for Design of Anchoring Systems for Deepwater Offshore Structures. Offshore Technology Conference,5 May-8 May 2003, Houston, Texas.

Garrett, C., and P. Cummins, 2005. The power potential of tidal currents in channels. Proceedings of Royal Society A, 461, 2563-2572.

Garrett, C., and P. Cummins, 2008. Limits to tidal current power, Renewable Energy, 33, 2485-2490.

Gooch, S., J. Thomson, B. Polagye, and D. Meggitt, 2009. Site Characterization for Tidal Power. Oceans 2009, Biloxi, MI, October 26-29, 2009.

Johnson, G.L., 1985. Wind energy systems. New York, USA: Prentice Hall.

Kawase, M. and K.M. Thyng, 2010. Three-dimensional Hydrodynamic Modelling of Inland Marine Waters of Washington State, United States, for Tidal Resource and Environmental Impact Assessment, IET Renewable Power Generation, accepted.

Maas, L.R.M., and J.J.M. Van Haren, 1987. Observations on the vertical structure of tidal and inertial currents in the central North Sea. Journal of Marine Research, 45(2), 293-318.

Moore, S.K., N. Mantua, M. Kawase, J.A. Newton, M.J. Warner and J.P. Kellogg, 2008. A descriptive analysis of temporal and spatial patterns of variability in Puget Sound oceanographic properties. Estuarine, Coastal and Shelf Sciences, 80, 545–554.

Polagye, B., P. Malte, M. Kawase, and D. Durran, 2008. Effect of large-scale kinetic power extraction on time-dependent estuaries, Proceedings of the Institution of Mechanical Engineers, Part A, Journal of Power and Energy, 222, 471–484.

Polagye, B., M. Kawase and P. Malte, 2009. In-Stream Tidal Energy Potential of Puget Sound, Washington. Proceedings of the Institution of Mechanical Engineers, Part A, Journal of Power and Energy, 223, 571-587.

Prandle, D., 1982a. The vertical structure of tidal currents and other oscillatory flows. Continental Shelf Research, Volume 1(2), 191-207.

Prandle, D., 1982b. The vertical structure of tidal currents, Geophysical and Astrophysical Fluid Dynamics, 22, 29–49.

Proudman, J., 1953. Dynamical Oceanography, Methuen, London.

Simpson, J., and A. Souza, 1995, Semidiurnal switching of stratification in the region of freshwater influence of the Rhine, Journal of Geophysical Research, 100(C4), 7037-7044.

Spera, D. A., and T. R. Richards, 1979. Modified Power Law Equations for Vertical Wind Profiles, in Conference and Workshop on Wind Energy Characteristics and Wind Energy Siting 1979, Portland, Oreg., June 1979, Pacific Northwest Laboratory, Battelle Memorial Institute, Report PNL-3214.

Strickland, R.M., 1983. The Fertile Fjord: Plankton in Puget Sound. Washington Sea Grant, Seattle.

Weyman, E., 2006. Coupled Dynamics and Economic Analysis of Floating Wind Turbine Systems. M.S. Thesis, Massachusetts Institute of Technology.

Disclaimer

This report was prepared as an account of work sponsored by an agency of the United States Government. Neither the United States Government nor any agency thereof, nor any of their employees, makes any warranty, expressed or implied, or assumes any legal liability or responsibility for the accuracy, completeness, or usefulness of any information, apparatus, product, or process disclosed, or represents that is use would not infringe privately owned rights. Reference herein to any specific commercial product, process, or service by trade name, trademark, manufacturer, or otherwise does not necessarily constitute or imply its endorsement, recommendation, or favoring by the United States Government or any

agency thereof. Their views and opinions of the authors expressed herein do not necessarily state or reflect those of the United States Government or any agency thereof.

Table 1. List of ADCP data used for this study

Name	**Latitude Longitude**	**Start – End**	**ADCP**	**Bins**	**Bin Size**	**Bin Range**
2007 Admiralty Head (AH07)	48° 8’ 53.034” N 122° 42’ 0.048” W	08/18/2007 10:15:00 – 09/19/2007 13:15:00	300 kHz RDI	38	2m	3.8-77.8 m
2007 Point Wilson (PW07)	48° 8’ 59.772” N 122° 42’ 53.898” W	08/18/2007 10:45:00 – 09/19/2007 12:30:00	500 kHz SonTek	68	1m	2-96m
2009 Admiralty Head (AH09)	48° 9’ 7.5594” N 122° 41’ 43.44” W	04/09/2009 05:10:00 – 05/19/2009 11:30:00	307.2 kHz Broadband	79	1m	3.57-81.57m
2008 Marrowstone Island C5	48° 6’ 32.4” N 122° 41’ 8.5194” W	11/13/2008 15:03:00 – 12/16/2008 09:48:59	307.2 kHz Broadband	25	1m	5.21-29.21m
2008 Marrowstone Island D9	48° 2’ 16.0794” N 122° 39’ 43.9194” W	11/13/2008 13:42:00 – 12/16/2008 10:34:00	614.4 kHz Broadband	26	1m	4.1-29.1m
2008 Marrowstone Island D10	48° 2’ 5.9994” N 122° 39’ 42.4794” W	11/13/2008 13:58:00 – 12/16/2008 10:45:00	614.4 kHz Broadband	23	1m	4.1-26.1m
2008 Marrowstone Island D11	48° 1’ 55.1994” N 122° 39’ 40.3194” W	11/13/2008 13:51:00 – 12/16/2008 10:54:00	307.2 kHz Broadband	21	1m	5.21-25.21m

Table 2. The best fit exponent γ for a power law profile $\overline{P} \sim z^{\gamma}$ for power density calculated from ADCP observations

Name	**γ, Bottom Boundary Layer, F_C = 30%/35%**	**Maximum Height of Bottom Boundary Layer**	**γ, Above Bottom Boundary Layer, F_C = 30%/35%**
2007 Admiralty Head (AH07)	0.6157/0.6165	18m	0.4172/0.4311
2007 Point Wilson (PW07)	0.6213/0.6373	21m	0.1890/0.2030
2009 Admiralty Head (AH09)	0.3542/0.3505	32m	0.4919/0.5040
2008 Marrowstone Island C5	0.9146/0.9610		
2008 Marrowstone Island D9	0.6552/0.6572		
2008 Marrowstone Island D10	0.6503/0.6540		
2008 Marrowstone Island D11	0.6224/0.6212		

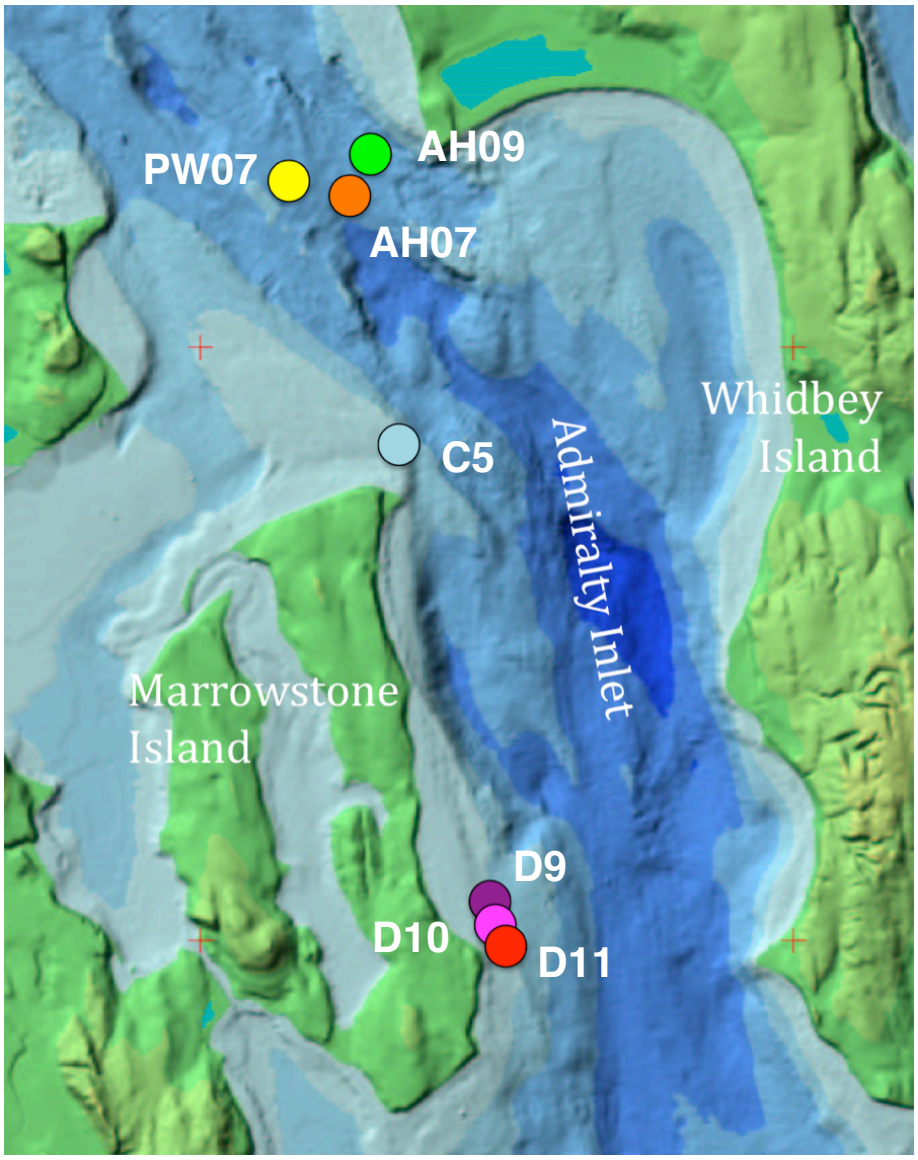

Figure 1. Admiralty Inlet, Washington, with locations of the ADCP installtions whose data are used in this study.

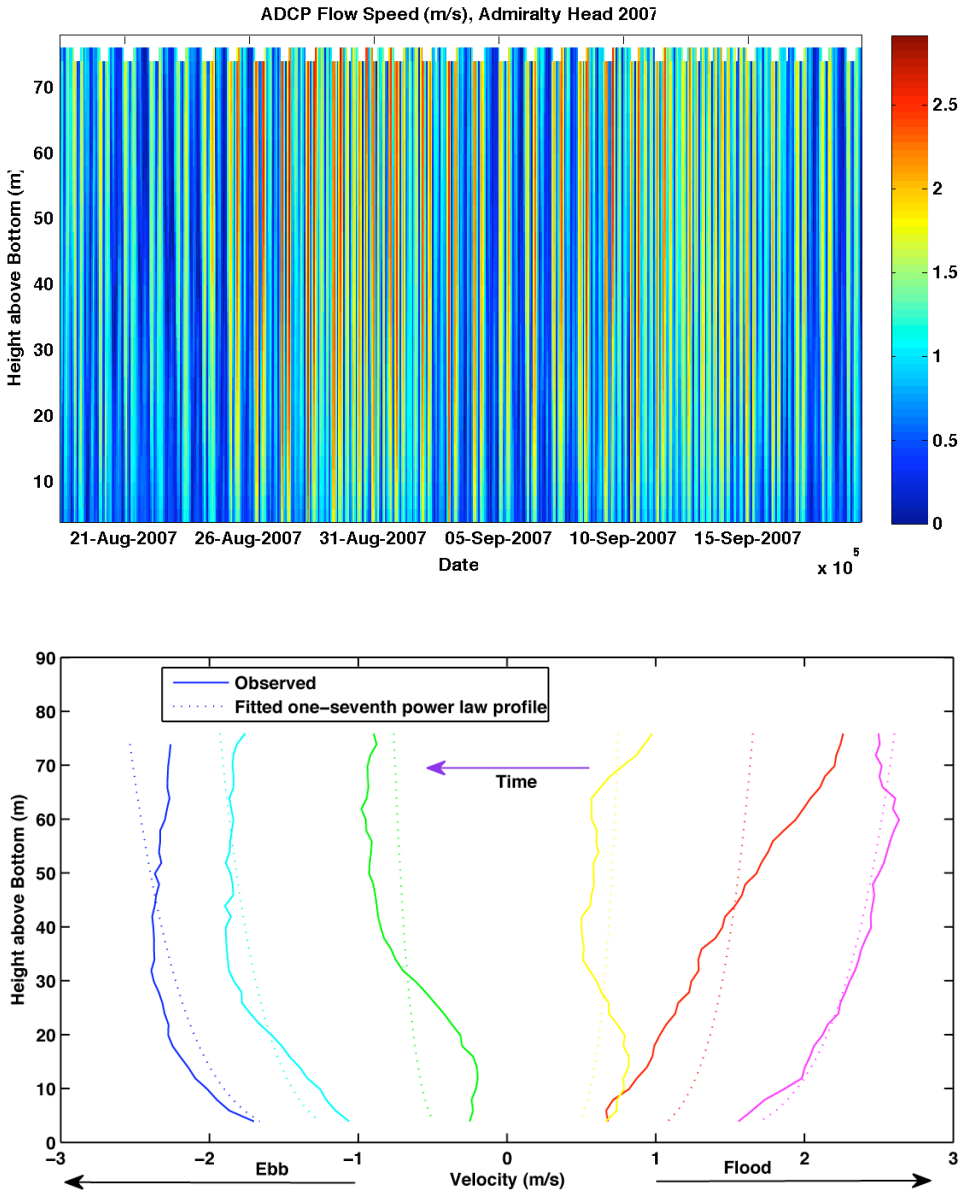

Figure 2. (Top) Flow speed (in meters per second) from the Admiralty Head 2007 (AH07) ADCP data. See Figure (1) for the location. (Bottom) Vertical current profiles (every thirty minutes) from peak flood to peak ebb during a typical tidal cycle at AH07. For each profile, a corresponding one-seventh power law profile with the same vertically averaged speed is shown with a dotted line.

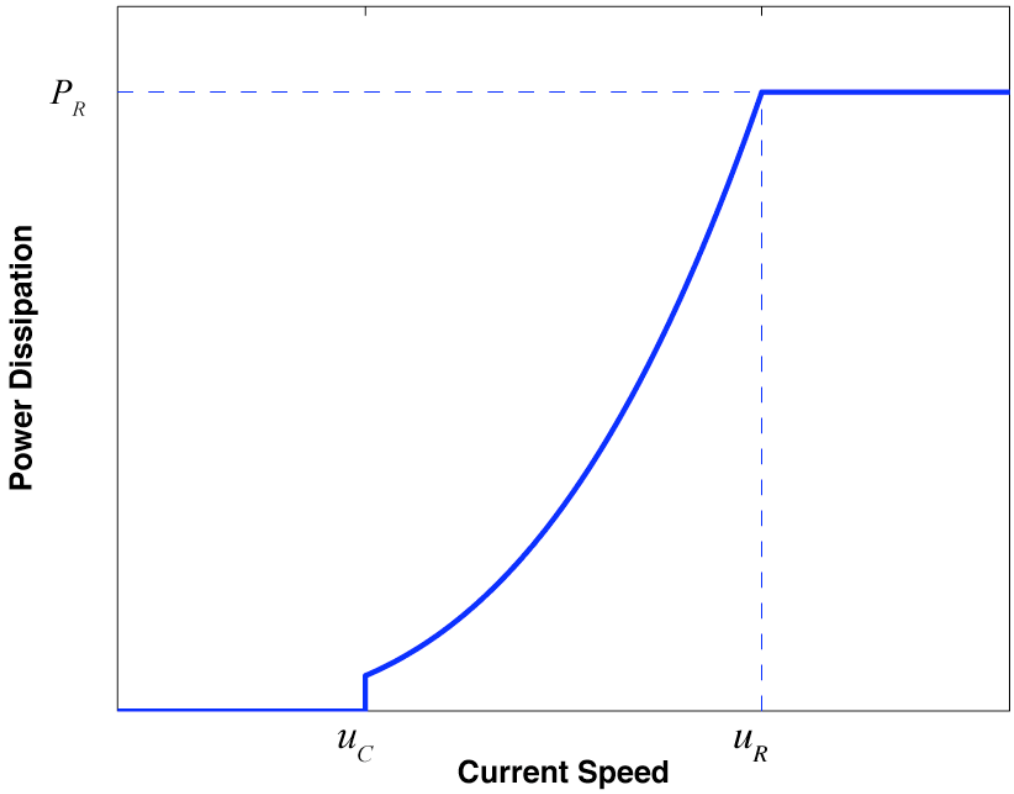

Figure 3. Speed-power relationship Equation (1) used in this study.

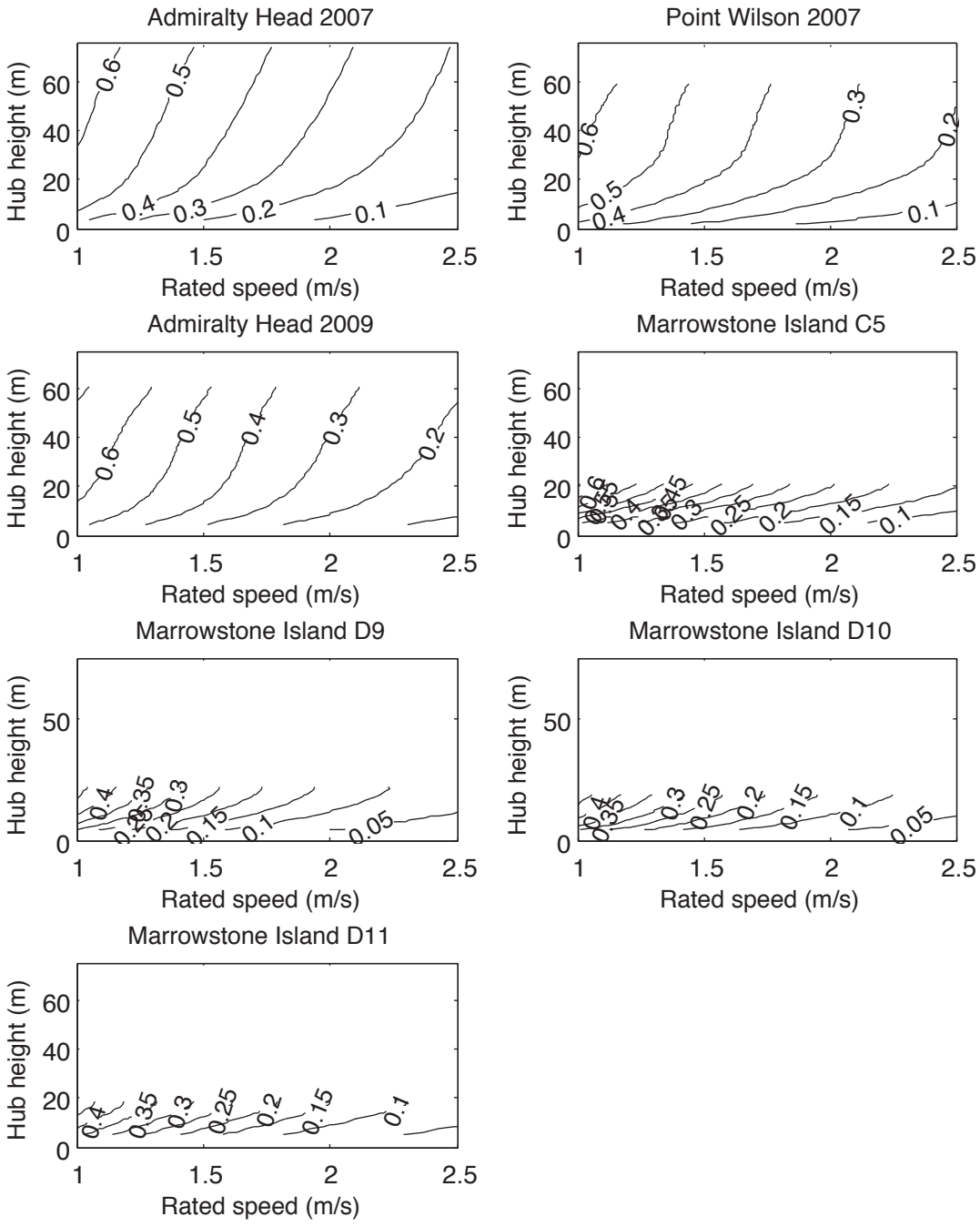

Figure 4. Capacity factor F_C as a function of rated speed u_R and hub height above sea bottom.

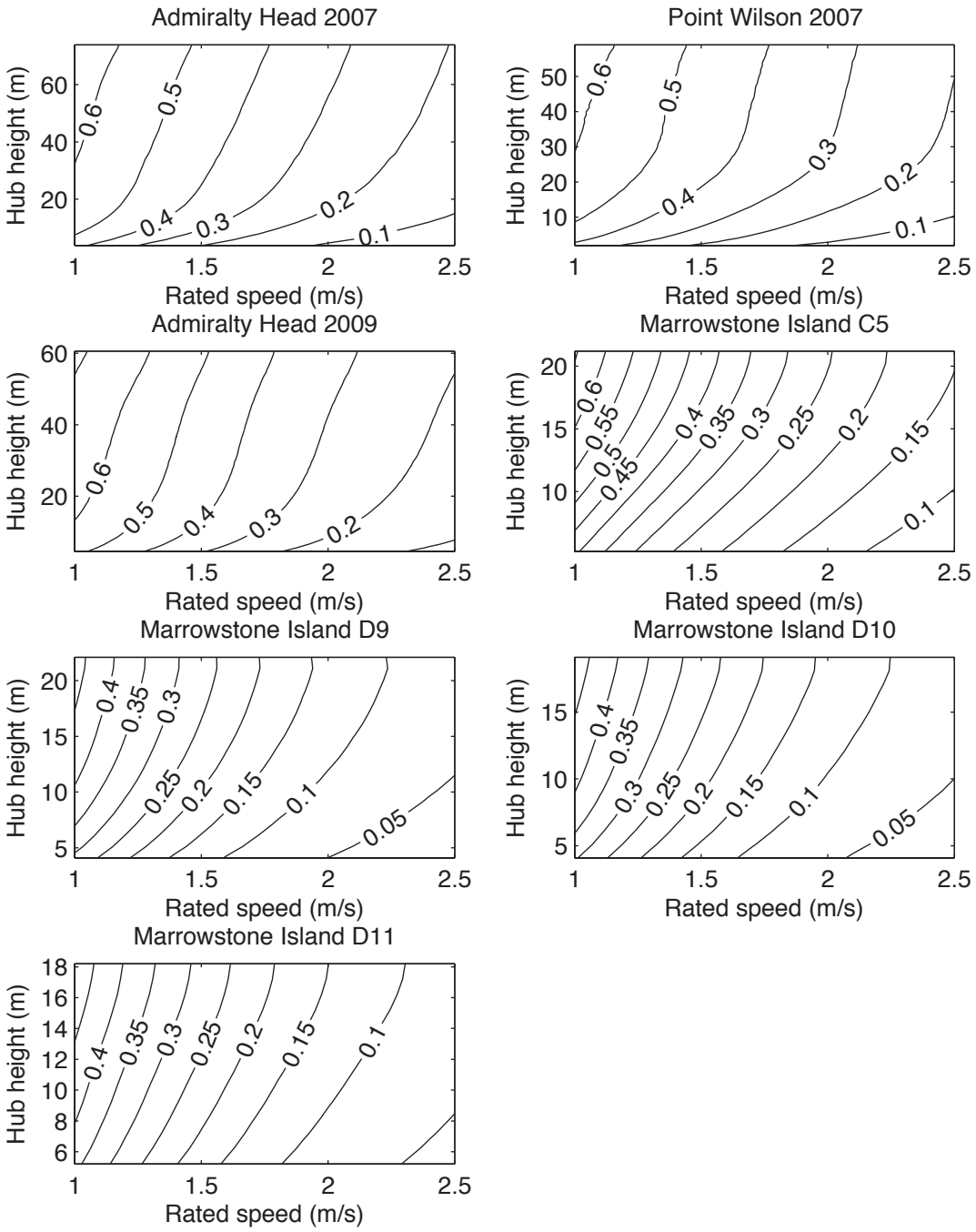

Figure 5. As in Figure 4, but the vertical axes are rescaled to fit each plot to the figure window.

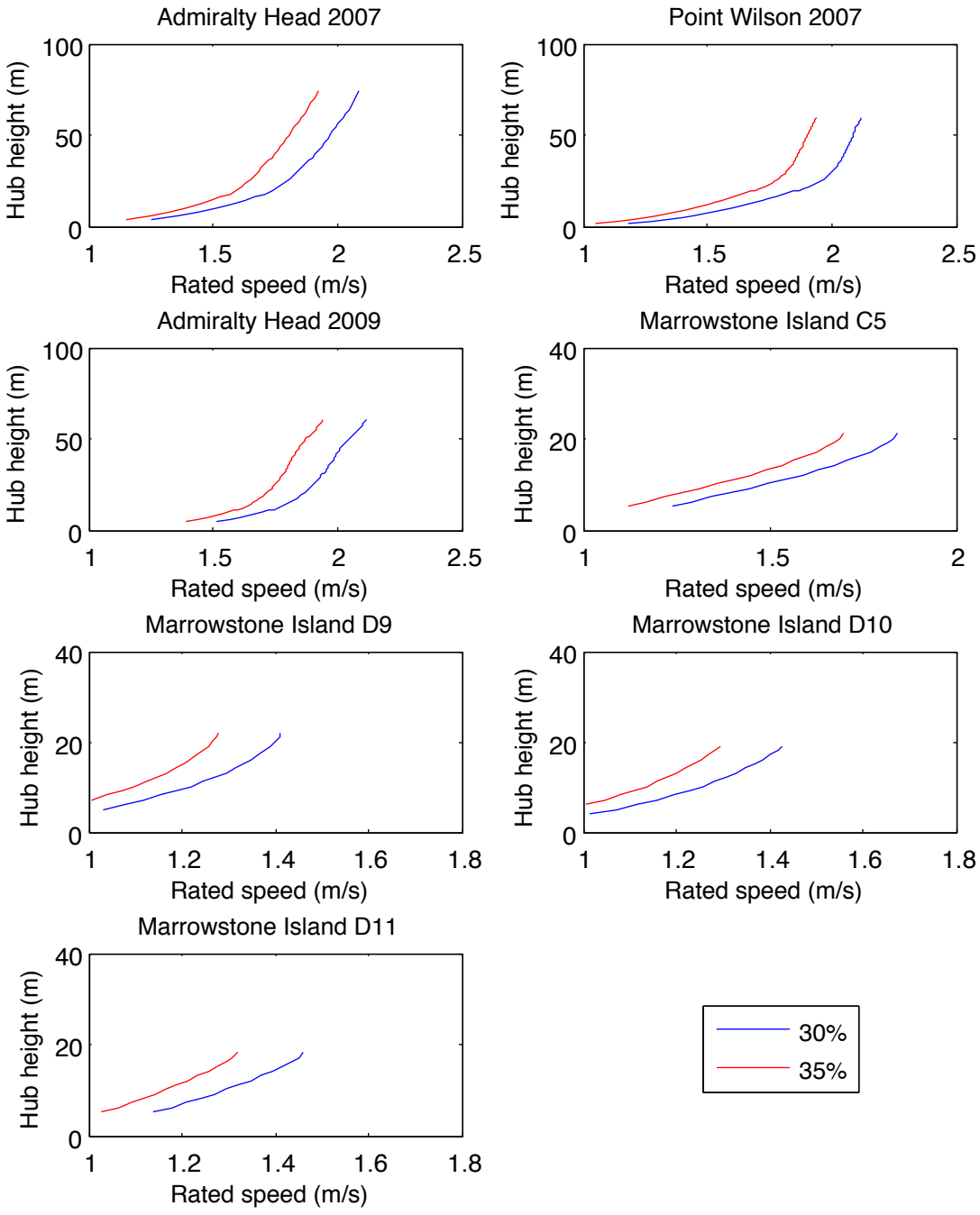

Figure 6. Rated speeds for capacity factors of 30% and 35% as a function of hub height above sea bottom.

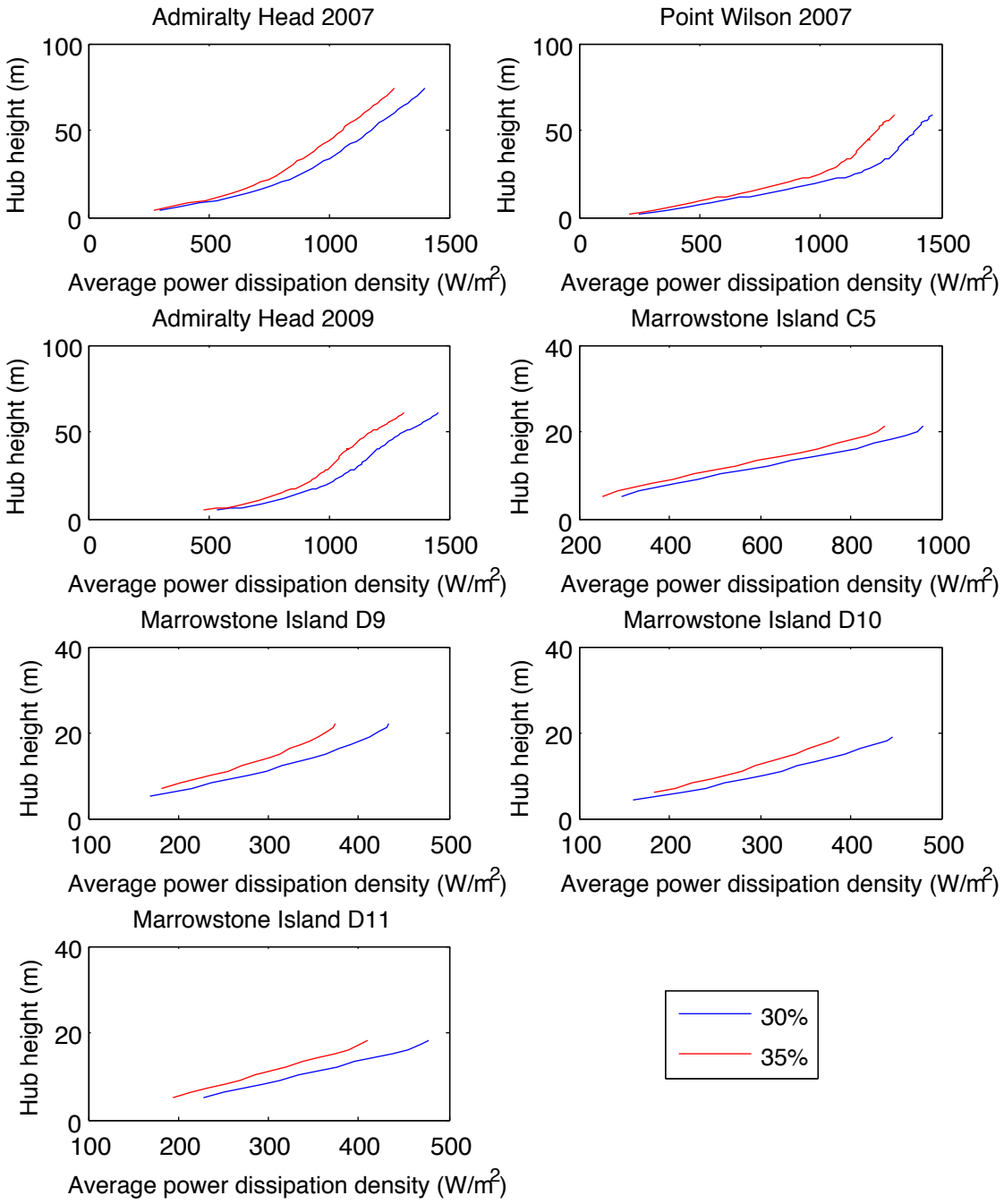

Figure 7. Average power dissipation density for capacity factors of 30% and 35% as a function of hub height above sea bottom.

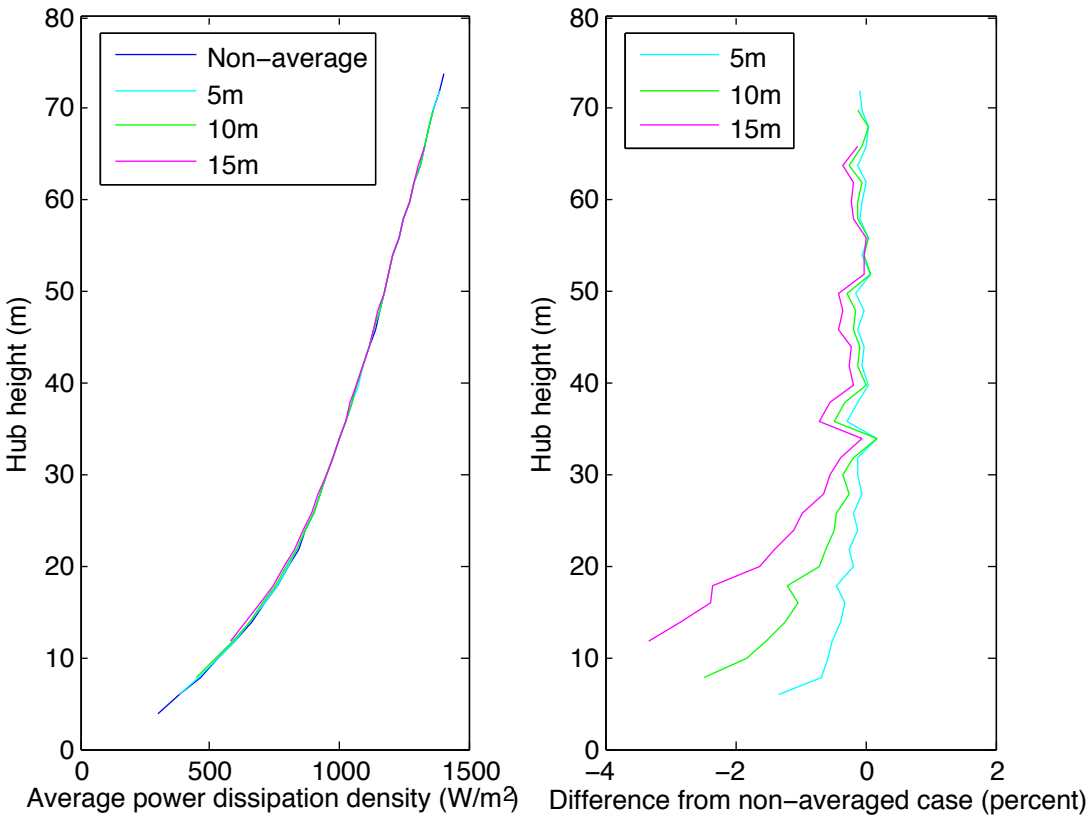

Figure 8. Comparison of power dissipation densities calculated from raw (non-averaged) speed and speeds averaged across the face of turbines of diameters 5, 10 and 15 meters. Left: average power dissipation density. Right: relative difference between the averaged and non-averaged cases.

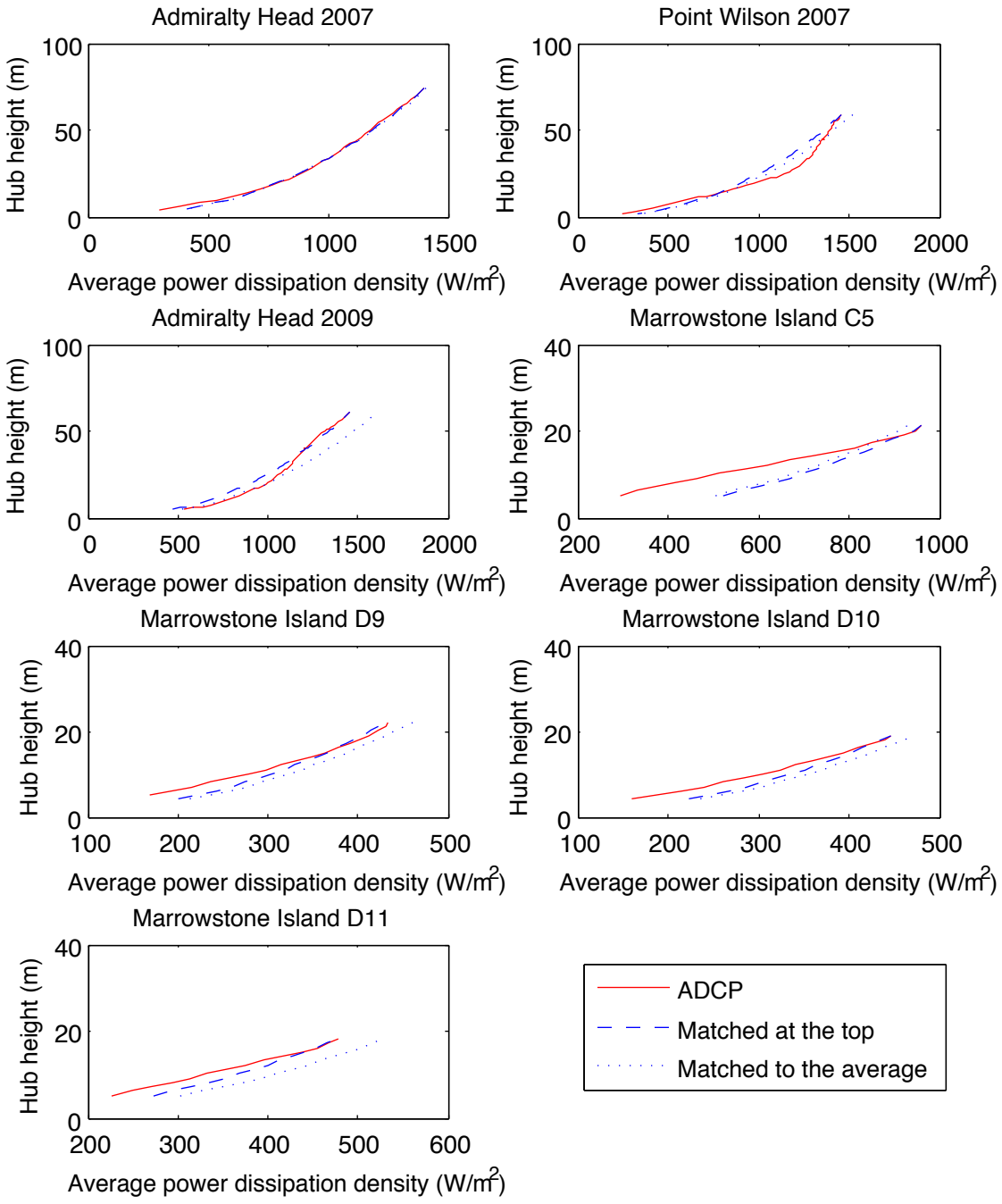

Figure 9. Average power dissipation density for a capacity factor of 30%, calculated from the ADCP data (red), one-seventh law profile matched to the ADCP data at the top (blue dashed), and one-seventh law profile matched to ADCP in the vertical average (blue dotted).

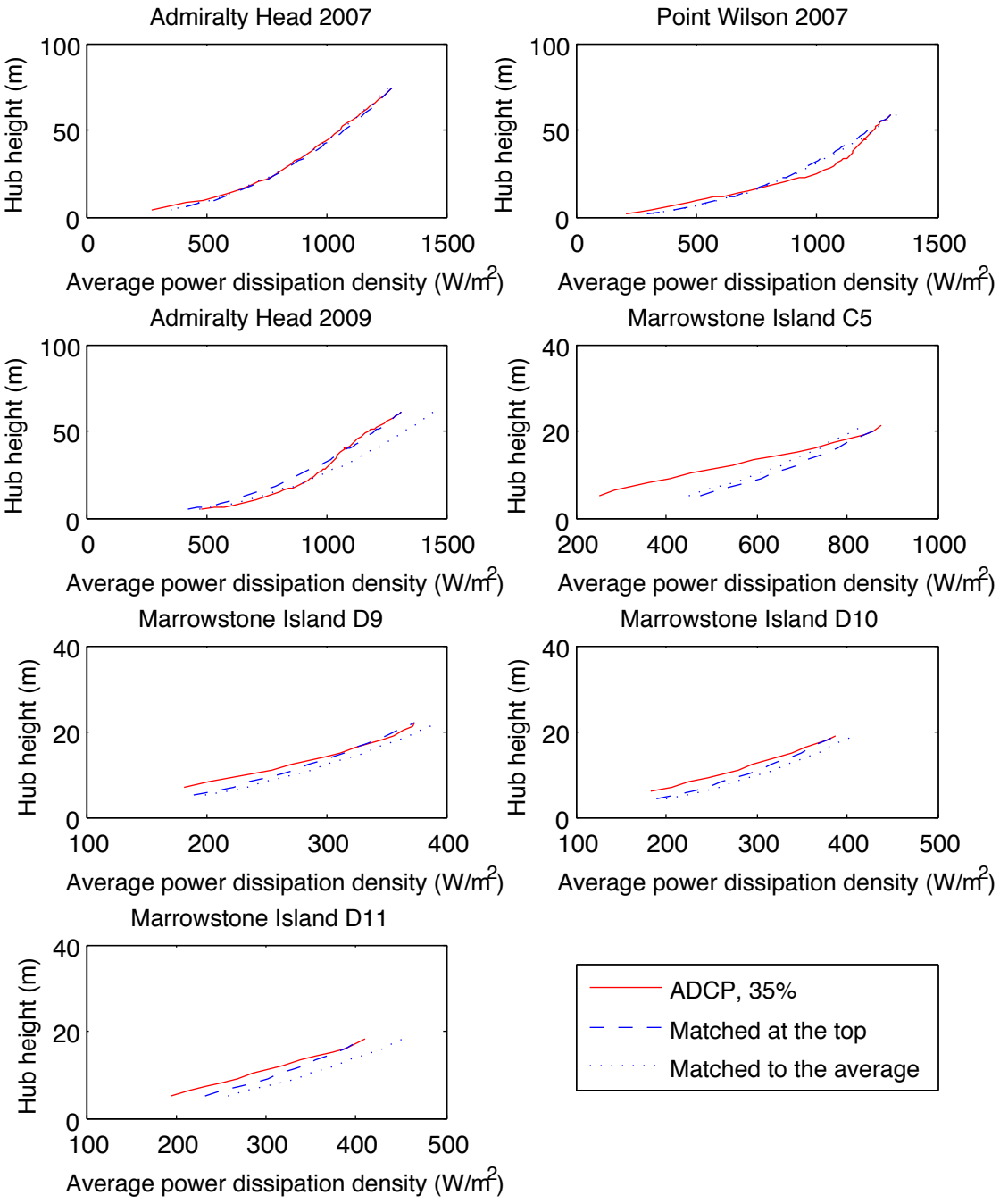

Figure 10. As in Figure 9, but for a capacity factor of 35%.

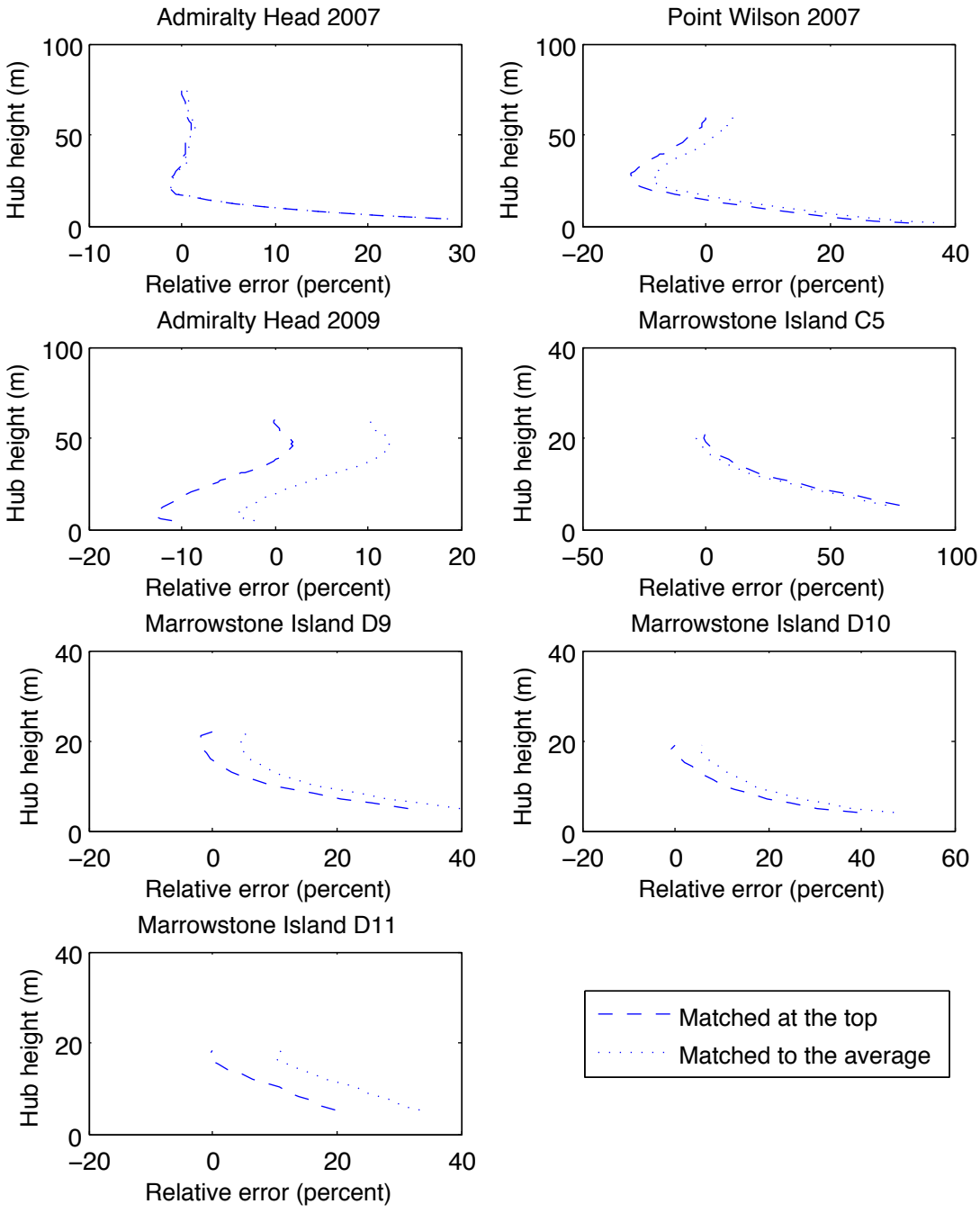

Figure 11. Percent error of average power calculation for a capacity factor of 30% using the one-seventh law (see Fig.9), matched to the ADCP data at the top (dashed), in the vertical average sense (dotted), relative to the ADCP-based calculation.

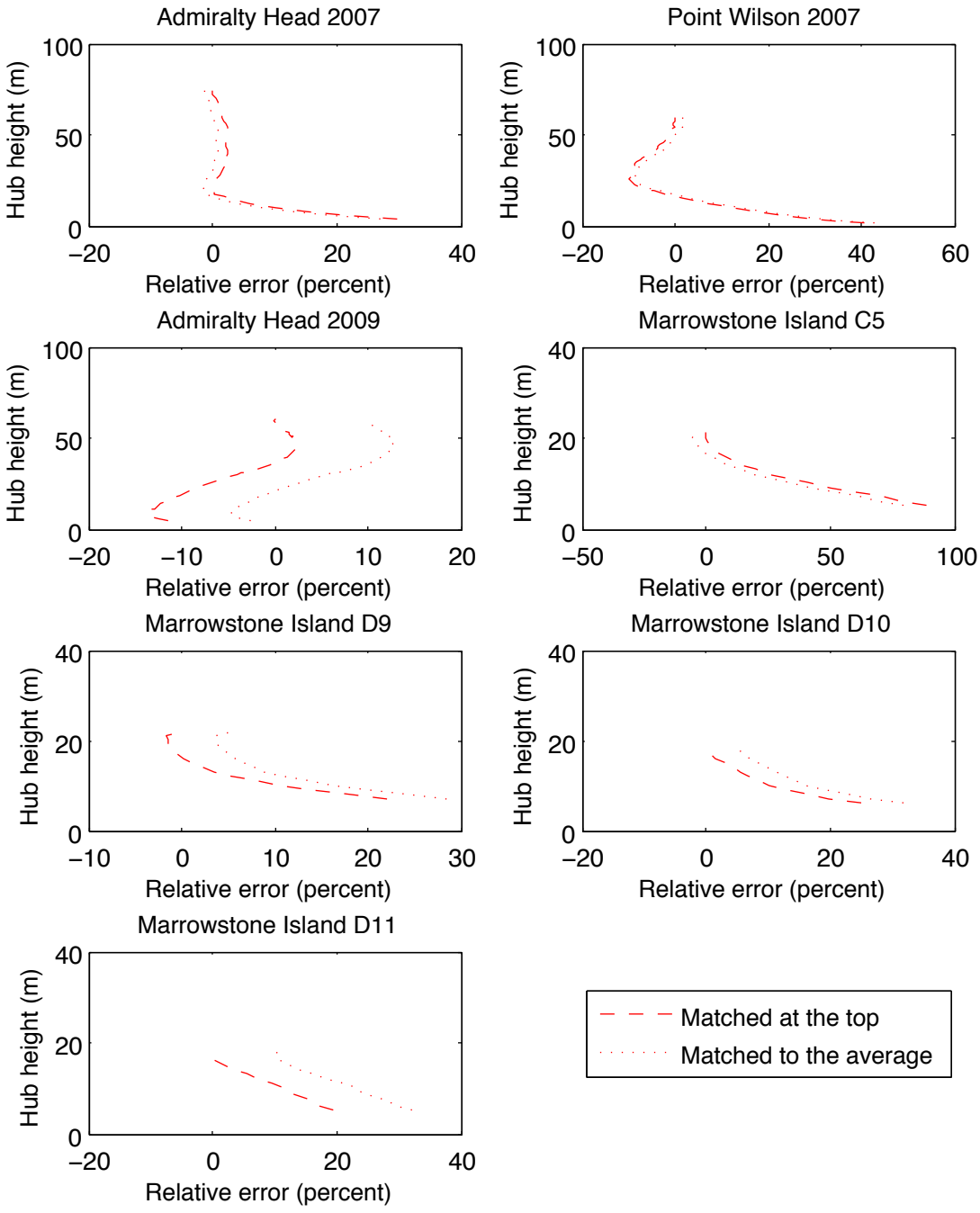

Figure 12. As in Figure 11 but for a capacity factor of 35% (see Fig.7).

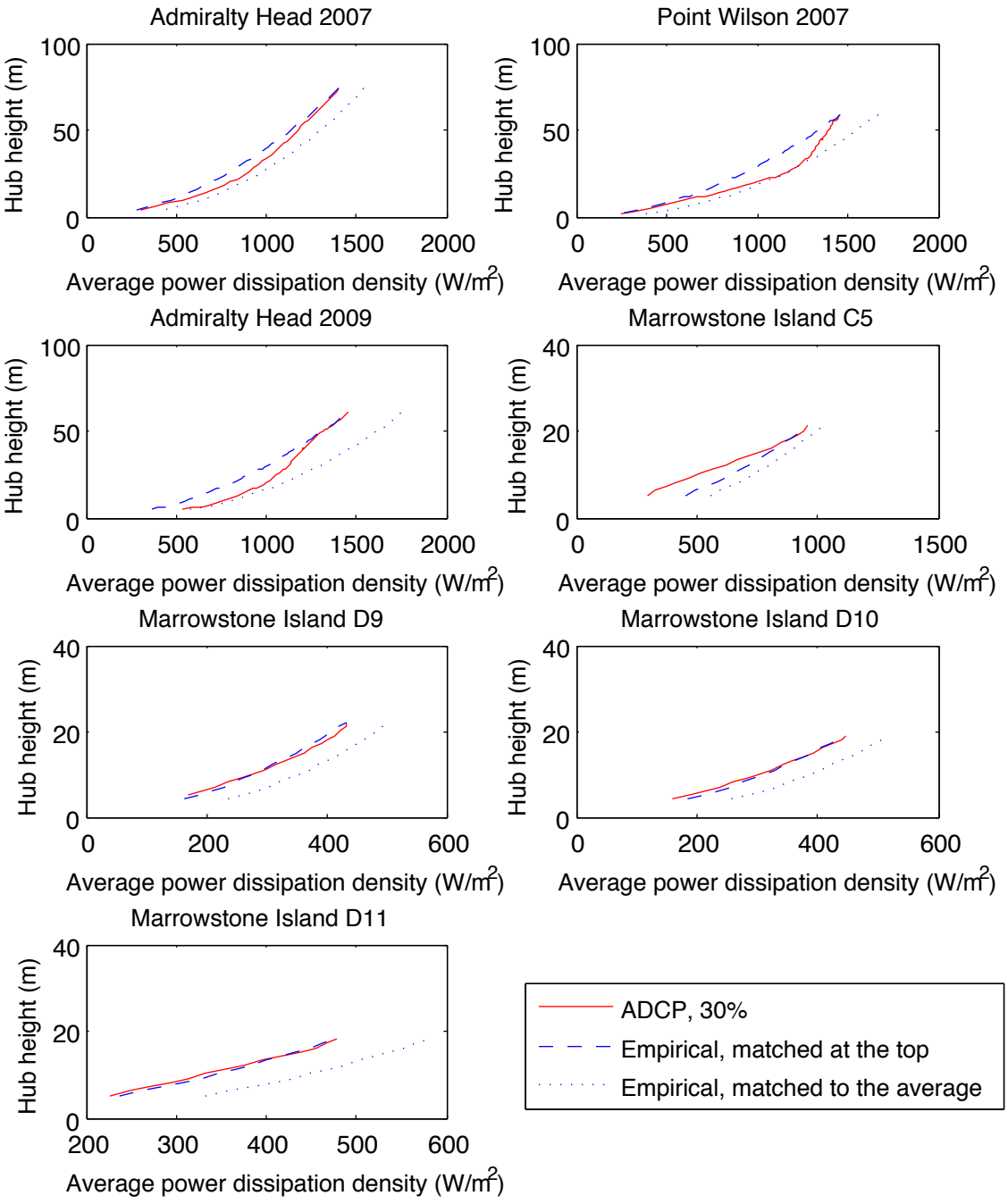

Figure 13. As in Figure 9, but with an empirical power law profile of $\gamma = 0.177$.

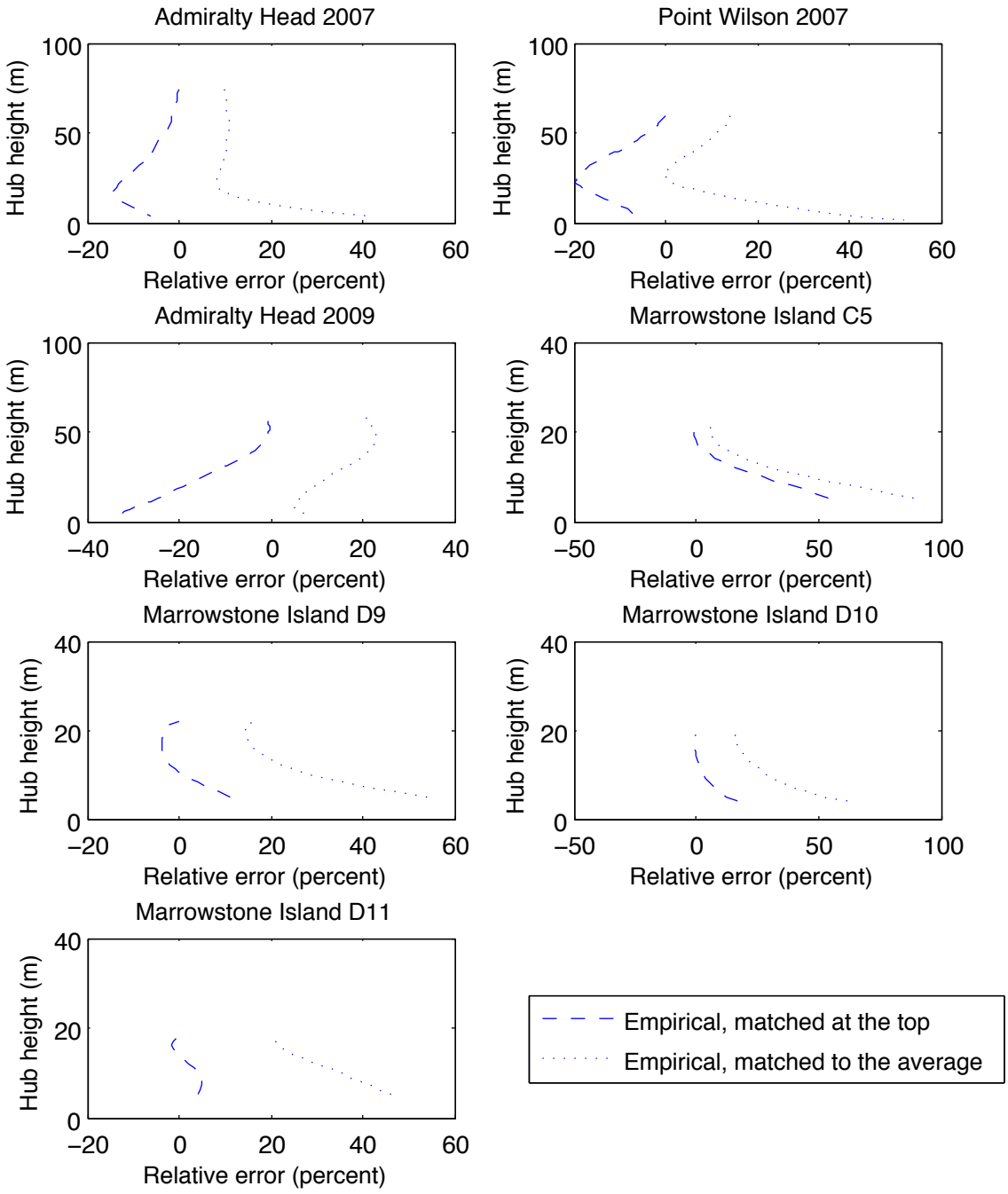

Figure 14. As in Figure 11, but with an empirical power law profile of $\gamma = 0.177$.

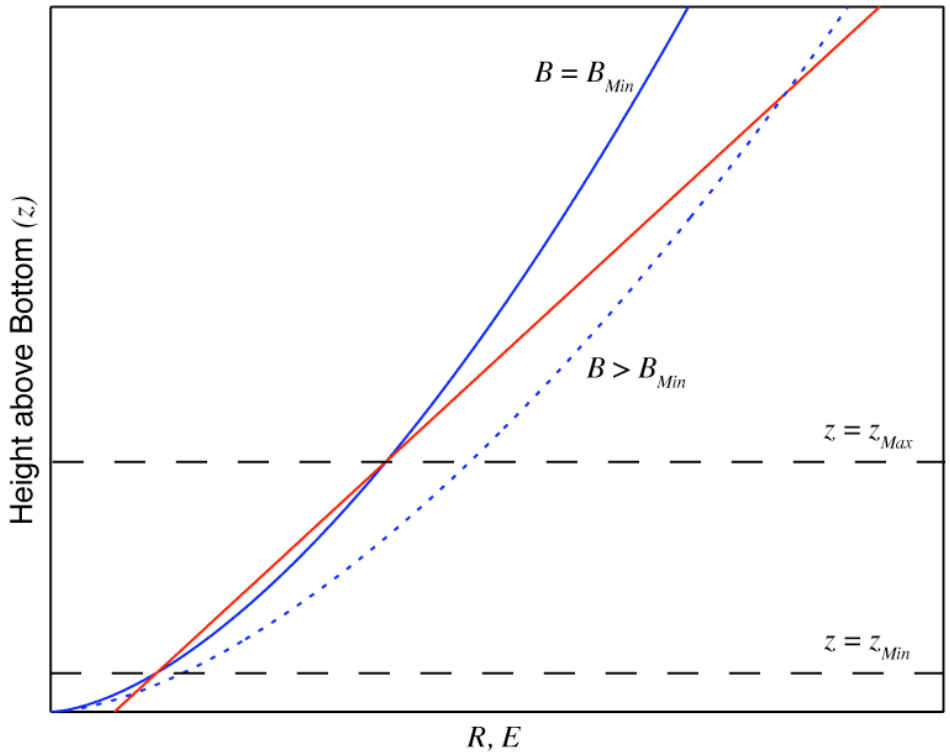

Figure 15. Schematic plot illustrating how an optimal height above bottom for a tidal turbine may be determined. Red line indicates total cost of installation as a function of height above bottom; solid blue line indicates total revenue for the minimum average price of electricity. Intersections of two lines bracket the depth range for assured profit. Dotted blue line is total revenue for an average electricity price higher than the expected minimum. Note the extra profit margin is greater if the device is placed higher in the profitable range.